Atmos. Chem. Phys. Discuss., 15, 18537–18576, 2015
www.atmos-chem-phys-discuss.net/15/18537/2015/
doi:10.5194/acpd-15-18537-2015

Atmospheric Chemistry and Physics Discussions

New characteristics of submicron aerosols and factor analysis of combined organic and inorganic aerosol mass spectra during winter in Beijing

J. K. Zhang, D. S. Ji, Z. R. Liu, B. Hu, L. L. Wang, X. J. Huang, and Y. S. Wang

State Key Laboratory of Atmospheric Boundary Layer Physics and Atmospheric Chemistry (LAPC), Institute of Atmospheric Physics, Chinese Academy of Sciences, Beijing 100029, China

Received: 22 April 2015 – Accepted: 11 June 2015 – Published: 08 July 2015

Correspondence to: Y. S. Wang (wys@mail.iap.ac.cn)

Published by Copernicus Publications on behalf of the European Geosciences Union.

Abstract

In recent years, an increasing amount of attention has been paid to heavy haze pollution in Beijing, China. In addition to Beijing's population of approximately 20 million and its 5 million vehicles, nearby cities and provinces are host to hundreds of heavily polluting industries. In this study, a comparison between observations in January 2013 and January 2014 showed that non-refractory PM_1 (NR-PM_1) pollution was weaker in January 2014, which was primarily caused by variations in meteorological conditions. For the first time, positive matrix factorization (PMF) was applied to the merged high-resolution mass spectra of organic and inorganic aerosols from aerosol mass spectrometer measurements in Beijing, and the sources and evolution of NR-PM_1 in January 2014 were investigated. The two factors, NO_3-OA1 and NO_3-OA2, were primarily composed of ammonium nitrate, and each showed a different degree of oxidation and diurnal variation. The organic fraction of SO_4-OA showed the highest degree of oxidation of all PMF factors. The hydrocarbon-like organic aerosol (OA) and cooking OA factors contained negligible amounts of inorganic species. The coal combustion OA factor contained a high contribution from chloride in its mass spectrum. The NR-PM_1 composition showed significant variations in January 2014, in which the contribution of nitrate clearly increased during heavy pollution events. The most effective way to control fine particle pollution in Beijing is through joint prevention and control measures at the regional level, rather than a focus on an individual city, especially for severe haze events.

1 Introduction

Particulate matter (PM) that is suspended in the atmosphere as atmospheric aerosols plays a crucial role in ambient visibility reduction, affects human health, and influences climate directly and indirectly by absorbing and reflecting solar radiation and modifying cloud formation (Watson, 2002; Charlson et al., 1992; Chow et al., 2006; IPCC, 2013).

ACPD
15, 18537–18576, 2015

Unfortunately, fine particle pollution in Beijing, the capital and one of the most economically developed regions of China, has increased significantly in recent years (Quan et al., 2011; Liu et al., 2013; Huang et al., 2014; Zheng et al., 2014a). Haze events associated with such pollution are much more frequent in winter, especially in January and December (Wang et al., 2014a). According to Huang et al. (2014), aerosol concentrations increased significantly in 2012–2013; compared to January 2011, aerosol optical depths increased by 0.16 and 0.43 in 2012 and 2013, respectively. The average $PM_{2.5}$ mass concentration was 89.5 $\mu g\,m^{-3}$ in 2013, which was 156 % larger than the first national environmental standard (35 $\mu g\,m^{-3}$) in China. The number of heavy pollution days (air quality index > 200; see Huang et al. (2014) for more details) reached approximately 58 in 2013, and the primary pollutants on all of these days belonged to the $PM_{2.5}$ fraction.

As reported by Zhang et al. (2014), the most serious PM pollution of this century in Beijing occurred in January 2013, when the highest instantaneous concentration of $PM_{2.5}$ reached 1000 $\mu g\,m^{-3}$ in some heavily polluted areas. Understanding the sources and processes responsible for PM composition and concentration is critical for the public to recognize the regional haze events over this megacity and for the government to enact effective PM reduction strategies (Liu et al., 2013).

At present, the most popular method for the apportionment of aerosol mass spectrometer (AMS) observation data is positive matrix factorization (PMF) (Paatero and Tapper, 1994; Ulbrich et al., 2009). After combining the organic mass fractions observed by the AMS, the organic aerosols (OA) can be decomposed into several sub-components, such as hydrocarbon-like OA (HOA), biomass burning OA (BBOA), cooking-related OA (COA), coal combustion OA (CCOA), and oxygenated organic aerosol (OOA). In addition, the OOA factor has been further separated into a low volatility fraction (LV-OOA) and a semi-volatile fraction (SV-OOA) in some studies. (Aiken et al., 2008; Huang et al., 2011; Mohr et al., 2012; Zhang et al., 2014). These OA factors show variation in characteristics such as hygroscopicity, volatility, oxidation states,

ACPD
15, 18537–18576, 2015

formation pathways and sources, which significantly improves our understanding of OA in the atmosphere (Jimenez et al., 2009).

However, we must note that other carbonaceous and inorganic species account for a significant fraction of the PM_1 mass. Therefore, a PMF analysis focused on OA spectra alone may hide the intrinsic relationship between organic and inorganic species and neglect the inherent links between them. Fortunately, some alternative and innovative approaches have recently been used that take advantage of PMF analyses including these species. For example, Sun et al. (2012b) performed the first PMF analysis on combined organic and inorganic aerosol HR mass spectra from high-resolution aerosol mass spectrometer (HR-ToF-AMS) measurements. They identified eight factors, but only five factors were resolved when accounting for only OA. They concluded that the combined analysis provided more useful information on the non-refractory PM_1 (NR-PM_1) than analyses focused on OA spectra alone. More recently, McGuire et al. (2014) performed PMF analysis on AMS full particle-phase mass spectra and compared the results to analysis of only the organic mass spectra. They found that the full particle-phase mass spectrum method enabled additional conclusions to be drawn regarding aerosol sources and chemical processes. Furthermore, by combining the high-resolution OA and SO_4^{2-} spectra, Crippa et al. (2013) identified a new emissions type, marine OA (MOA), alongside the common LV-OOA, SV-OOA, HOA, and COA. These novel methodologies are therefore of great interest for an improved understanding of pollution sources and their evolution in the atmosphere.

Unfortunately, there are few studies that have used this innovative approach to analyze AMS mass spectra, and there has been no work of this kind conducted in China, despite the serious fine particle pollution and frequent heavy pollution events in this country. Therefore, in the present study, we deployed a high-resolution time-of-flight AMS (for convenience, we refer to this instrument simply as the AMS), manufactured by Aerodyne Research Inc. (Billerica, MA, USA) in urban Beijing to measure airborne submicron particles at a high temporal resolution during January of 2014. We then performed the following analyses: (1) comparison of the difference in NR-PM_1 in similar

ACPD
15, 18537–18576, 2015

periods in 2013 and 2014, (2) integration of organic and inorganic HR spectral matrices into one unified dataset for PMF analysis based on the method of Sun et al. (2012b) (to the best of our knowledge, this is the first time PMF analysis based on both organic and inorganic HR spectral matrices has been applied in Beijing) and evaluation of the evolution of PMF factors, and (3) analysis and comparison of the characteristics of the heavy haze events that occurred in January 2013 and 2014.

2 Experimental methods

2.1 Sampling site

Online measurements of the NR-PM_1 aerosol species were performed continuously between 1 January and 3 February 2014, at the same location as Zhang et al. (2014); namely, the Institute of Atmospheric Physics, Chinese Academy of Sciences. The observation site is located between the north 3rd Ring Road and north 4th Ring Road. The site is approximately 1 km from the 3rd Ring Road, 200 m from the Badaling Highway running north–south to its east, and 50 m from the Beitucheng West Road running east–west to its north (Fig. S1). Ambient air was sampled at approximately 10 m above the ground.

In addition to AMS deployment, the total PM_1 mass concentration was simultaneously monitored at hourly intervals using a beta-attenuation method (Metone BAM-1020, USA), and the results are appropriate for comparison with those of the AMS. Meteorological parameters, including temperature (T), relative humidity (RH), wind speed (WS), wind direction (WD), and air pressure were observed from an automatic meteorological observation instrument (Milos520, Vaisala, Finland). Commercial instruments from Thermo Fisher Scientific (TE), USA, were used to measure O_3 (model 49I), $NO/NO_2/NO_x$ (model 42I), CO (model 48I) and SO_2 (model 43I). Detailed information about these instruments, such as their setups, calibration and operation and maintenance have been described in detail by Ji et al. (2012).

ACPD
15, 18537–18576, 2015

2.2 Instrumentation and data analysis

2.2.1 HR-ToF-AMS operation

Detailed descriptions of the Aerodyne AMS have been presented in many previous publications and reviewed by DeCarlo et al. (2006) and Canagaratna et al. (2007). Similar operational methods were used in January 2013 and 2014; in both cases, the AMS was operated under both the "V" and "W" ion optical modes, alternating every 7.5 min. Under V-mode operation, the AMS cycled through the mass spectrum (MS) mode and the particle ToF (PToF) mode every 45 s, spending 22.5 s in both its open and closed statuses under the MS mode. Following standard protocols, the AMS was calibrated for inlet flow, ionization efficiency (IE), and particle sizing at the beginning, middle and end of the campaign (Jayne et al., 2000; Jimenez et al., 2003; Drewnick et al., 2005). IE calibration was conducted using size-selected pure ammonium nitrate particles, and particle size calibration was conducted using mono-disperse polystyrene latex spheres. The detection limit of each individual species was determined as three times the standard deviation of the corresponding signal in particle-free air (DeCarlo et al., 2006; Sun et al., 2009). As a result, the 7.5 min detection limits of organics, sulfate, nitrate, ammonium, and chloride were 0.053, 0.008, 0.005, 0.029 and 0.012 $\mu g\,m^{-3}$, respectively.

2.2.2 HR-ToF-AMS data analysis

The mass concentrations and size distributions of the species measured with the AMS were calculated using the methods outlined in DeCarlo et al. (2006). The standard ToF-AMS data analysis software packages, SQUIRREL version 1.50 and PIKA version 1.09, both downloaded from the ToF-AMS-Resources webpage (http://cires.colorado.edu/jimenez-group/ToFAMSResources), were used to generate unit and high-resolution mass spectra from the V-mode and W-mode data, respectively (Huang et al., 2010; He et al., 2011). In this study, the collection efficiency (CE) was calculated according to the suggestions by Middlebrook et al. (2012). We found that the effects of

ACPD
15, 18537–18576, 2015

particle-phase water and ammonium nitrate could be neglected because a silica gel diffusion dryer was introduced and the mass fraction of ammonium nitrate (ANMF) was normally below 0.4 (Fig. S2). Therefore, the CE was mainly driven by aerosol acidity, and the relationship between CE and aerosol acidity could be parameterized as $CE_{dry} = \max(0.45, 1.0–0.73\ (NH_4/NH_{4,predict}))$ (Middlebrook et al., 2012). Due to the observation of high-acidity aerosols in this study (Fig. S3), variable CEs calculated using the above equation were applied. The relative ionization efficiency (RIE) values used in this study were 1.2 for sulfate, 1.1 for nitrate, 1.3 for chloride, and 1.4 for organics (Jimenez et al., 2003). An RIE value of 4.2 was used for ammonium based on the measurement of pure NH_4NO_3 particles.

PMF analyses (Paatero and Tapper, 1994) were performed on the high-resolution mass spectra (HRMS) using the PMF Evaluation Toolkit v2.05 (Ulbrich et al., 2009). The HRMS data and error matrices were generated as outlined in Allan et al. (2003) and Ulbrich et al. (2009). We considered only ions up to m/z 120, given that larger ions had a low S/N ratio and were biased as a result of insufficient mass resolution. Isotopes were systematically constrained in PIKA, but they were subsequently removed from the data and error matrices because their presence would have given excess weight to the parent ions in the PMF analysis (Setyan et al., 2012). Ions with an S/N ratio < 0.2 or between 0.2 and 2 were removed or downweighted by increasing their errors by a factor of 2 before the PMF analysis (Paatero and Hopke, 2003; Ulbrich et al., 2009). In addition, the particulate ion CO_2^+ and its associated CO^+, H_2O^+, HO^+, and O^+ were also downweighted according to Ulbrich et al. (2009). Both the HR data and error matrices were converted from ion signals to mass concentrations before PMF analysis. According to the method suggested by Sun et al. (2012b), the major fragment ions for each inorganic species (nitrate, sulfate, ammonium and chloride) were integrated with those of the OA into one unified dataset: NO^+ (m/z 30) and NO_2^+ (m/z 46) for nitrate; SO^+ (m/z 48), SO_2^+ (m/z 64), SO_3^+ (m/z 80), HSO_3^+ (m/z 81), and $H_2SO_4^+$ (m/z 98) for sulfate; NH^+ (m/z 15), NH_2^+ (m/z 16), NH_3^+ (m/z 17) for ammonium; and Cl^+ (m/z 35) and HCl^+ (m/z 36) for chloride. The sum of the selected fragment ions represented

ACPD
15, 18537–18576, 2015

the major fraction of nitrate (96.2 %), ammonium (99.6 %) and chloride (75.8 %) and approximately half of sulfate (50.6 %).

The PMF analysis was performed for 1 to 8 factors, and a detailed description of the evaluation process can be found in the Supplement (Discussion S1 and Fig. S4). Finally, the 6-factor, FPEAK = −0.1, seed = 0 solution was chosen as the optimal solution for our study.

All the data in this study are reported as Beijing local time which equals the Coordinated Universal Time (UTC) plus 8 h.

3 Results and discussion

3.1 Submicron aerosol characteristics in January 2013 and 2014

Several serious pollution events occurred during the January 2014 campaign, as expected based on the January 2013 data (Fig. 1a–c). Therefore, a wide range of NR-PM_1 mass concentrations was observed with values between 1.3 and 318 $\mu g\,m^{-3}$, and a mean mass concentration (average ±1 SD) of $50.5 \pm 47.8\,\mu g\,m^{-3}$. This value was lower than the mean mass concentrations of $66.8 \pm 55\,\mu g\,m^{-3}$ and $89.3 \pm 85.6\,\mu g\,m^{-3}$ in winter 2012 (Sun et al., 2013b) and 2013 (Zhang et al., 2014), respectively. This result was lower than the AMS observations recorded during summer in Beijing: 80.0 $\mu g\,m^{-3}$ in 2006 (Sun et al., 2010) and 61.1 $\mu g\,m^{-3}$ in 2008 (Huang et al., 2010). This value was also close to the mean value reported by Sun et al. (2012a) using Aerosol Chemical Speciation Monitor results (50 $\mu g\,m^{-3}$). However, compared to the mean concentration values observed in other cities worldwide, such as 11.0 $\mu g\,m^{-3}$ in New York City in 2009 (Sun et al., 2011) and 14.8 $\mu g\,m^{-3}$ in Pittsburgh in 2002 (Zhang et al., 2005a), the Beijing results are clearly at a substantially higher level. This indicates that fine particle pollution in Beijing remains very serious.

As shown in Figs. S5 and S6, there was a strong correlation between the PM_1 measured by the beta-attenuation method and the NR-PM_1 mass concentrations

ACPD
15, 18537–18576, 2015

(slope = 0.91, R^2 = 0.90), indicating that the AMS observations were reliable. The difference in mass concentrations between the two methodologies was primarily caused by differences in the measurement mechanisms of the two instruments.

Figures 1d and e compare the composition of NR-PM_1 between January 2013 and January 2014. The contribution of organics in January 2014 accounted for 54 % of the total mass, which was slightly higher than in January 2013. In contrast, the contribution of total inorganic species was reduced. This subtle difference in composition may be related to the lower strength and frequency of the heavy particle pollution events in January 2014 compared to January 2013. Many studies have shown that the contribution of organics will decrease with an increase in the NR-PM_1 mass concentration, whereas the contribution of inorganic species will increase (Zhang et al., 2014; Sun et al., 2014, 2013b). This suggests an enhanced role of secondary inorganic species in the formation of haze episodes. Some interesting changes were also observed in the contributions of inorganic species during the winter of 2014 (see Sect. 3.4).

The O/C atomic ratio of OA is an important parameter that is considered a good reference for the oxidation state and photochemical age of OA in the atmosphere (Jimenez et al., 2009; Ng et al., 2010). The mean O/C ratios (average ±1 SD) in January 2013 and January 2014 were 0.34±0.08 and 0.40±0.13, respectively, with a wider range (0.13–0.92) in January 2014 compared to January 2013 (0.14–0.58) (Fig. S7). This implies that there was a striking increase in the oxidation of OA in January 2014. In general, there are two primarily pathways for OA aging: (1) photochemical aging, associated with atmospheric oxidation agents such as O_3, and/or increased temperature, (2) aqueous-phase process aging, which corresponds closely to high RH in the atmosphere. Figure 2a and b showed that the O/C increased clearly with atmospheric temperature whereas the variations with RH were distinctly different in the two January observations. In January 2013, the O/C showed the similar increasing trend with RH as that with temperature whereas it exhibited a trend of first decrease (RH < 45 %) and then increase (RH > 45 %) with the RH in January 2014. Thus we can infer that the oxidation mechanism of OA was different when the RH was lower or higher than

ACPD
15, 18537–18576, 2015

45 % in January 2014. The OA aging was mainly caused by photochemical process when the RH was lower than 45 %, while it was dominated by aqueous-phase process when RH was higher than 45 %. The photochemical process can be proved by Fig. 2c, e and f, from which we can found that O/C increased evidently with the O_3 concentration (Fig. 2c), and the temperature and O_3 concentration both showed the highest values when the RH at low level (Fig. 2e and f) in January 2014. In January 2013, however, although the highest O_3 concentration appeared at low RH level (Fig. 2f), the temperature was at the lowest level (Fig. 2e). Which means the photochemical process was weak under this condition. This is the reason for the O/C was always lower than 0.4 and even showed a distinctly decrease with the increase of O_3 concentration in January 2013 (Fig. 2c). Then we can conclude that aqueous-phase process aging dominated the oxidation of OA in January 2013. However, the OA oxidation mechanisms in January 2014 not only contained the aqueous-phase process aging but also the photochemical process due to the elevated O_3 and temperature at low RH level. In addition, the O/C showed opposite trends with the increase of NR-PM_1 mass concentrations in the two January campaigns. It presented a "decrease-stable-decrease" trend with the increase of NR-PM_1 mass during January 2014 (Fig. 2d). However, the pattern of O/C varied with NR-PM_1 mass could be divided into three stages in January 2013: increased linearly when NR-PM_1 mass was lower than 125 $\mu g\,m^{-3}$; kept a stable and weak growth when NR-PM_1 mass ranged from 125 to 400 $\mu g\,m^{-3}$; remarkably increased when NR-PM_1 mass was higher than 400 $\mu g\,m^{-3}$. Above analysis suggested that the oxidation of aerosol in atmosphere is extremely complex, even for the same observation site and periods in adjacent years.

Particle acidity is a key parameter in the study of aerosols because it affects their hygroscopic growth, toxicity, and heterogeneous reactions (Sun et al., 2010). Calculation of the acidity of submicron aerosols uses NH_4^+ meas. / NH_4^+ pred., i.e., the ratio of the measured NH_4^+ concentration to the predicted NH_4^+ required to fully neutralize the measured SO_4^{2-}, NO_3^-, and Cl^- (Zhang et al., 2007). We found that the particle acidity in January 2014 was completely consistent with the results in January 2013; the slopes

ACPD
15, 18537–18576, 2015

were all 0.68 (Fig. S3) (Zhang et al., 2014). However, the contribution of three acidic components (SO_4^{2-}, NO_3^-, and Cl^-) to the total acidic compound content showed interesting variations due to the divergence of the NR-PM_1 composition in the two January studies. Figures 2g and h present the variations of the relative contributions of these three acidic components to the total acidic compound content and $NH_{4\,meas}^+$ as a function of the NR-PM_1 mass concentration in the two campaigns. An increasing trend in $NH_{4\,meas}^+$ with the aggravation of particle pollution was shown in both campaigns. However, there was a difference in the relative contributions of the three acidic components. Excluding the large variations in the lower NR-PM_1 mass concentration range, the contribution of sulfate showed a very stable and high value (~ 60 %), whereas nitrate and chloride stability was 30 and 10 % for January 2013, respectively. However, the contribution of nitrate and chloride showed a clear increase, especially for nitrate, and the contribution at the highest NR-PM_1 mass concentration range was even higher than for sulfate in January 2014. Consequently, the contribution of sulfate decreased steadily in response to increased particle pollution. In addition, the average contributions of sulfate, nitrate and chloride to the total acidic compound content were 57, 31, and 12 % in January 2013 and 48, 36, and 16 % in January 2014, respectively. This is in agreement with the higher contribution of nitrate to NR-PM_1 in January 2014, especially during the heavy pollution periods, which will be further discussed in Sect. 3.4.

3.2 Differentiation of NR-PM_1 components by PMF

Following consideration of several critical factors, such as the mass spectrum signatures, the correlation of time series with tracers, and diurnal cycles (Zhang et al., 2005b; Ulbrich et al., 2009), there were six factors identified in January 2014: NO_3-OA1, NO_3-OA2, SO_4-OA, COA, HOA, and CCOA. Figure 3 shows the mass spectrum profiles and time series for each of these factors. We must note that the O/C and OM/OC ratios shown in Fig. 3a were calculated only based on the organic signals in the MS of every factor. As mentioned in Sect. 2.2.2, the sum of the selected fragment ions account for 96.2 % of the total nitrate mass, 99.6 % of the total ammonium mass, 75.8 % of the

ACPD
15, 18537–18576, 2015

total chloride mass, and approximately half of sulfate (50.6 %). Thus the corresponding coefficients need to be applied for determining the mass of every inorganic species in each factor in this section. Taking nitrate as an example, the actual mass concentration of nitrate in factor 1 can be calculated by the following equation:

$$NO_{3\,\text{factor 1}}^{-} = (NO^{+}{}_{\text{factor 1}} + NO_{2\,\text{factor 1}}^{+})/0.962,$$

where $NO_{3\,\text{factor 1}}^{-}$ is the actual nitrate mass in factor 1, $NO^{+}{}_{\text{factor 1}}$ and $NO_{2\,\text{factor 1}}^{+}$ are the masses of NO^{+} and NO_2^{+} ions in factor 1, respectively, 0.962 means the selected NO^{+} and NO_2^{+} ions account for 96.2 % of the total nitrate mass. After calculation, we found that the six factors together accounted for 97.8 % of the total NR-PM_1 in January 2014. The mass concentration of each factor and their contributions to the total NR-PM_1 used in the following discussion were the results of calculation.

3.2.1 NO_3-OA1, NO_3-OA2 and SO_4-OA

Two NO_3-OA factors were identified in the present study, NO_3-OA1 and NO_3-OA2 (Fig. 3), compared with only one, NO_3-OA, identified by Sun et al. (2012b) and McGuire et al. (2014). The mass concentration and proportion of ammonium nitrate in NO_3-OA1 and NO_3-OA2 were clearly higher than in the other factors (Fig. 4a and b). The mass concentration and proportion were 7.4 $\mu g\,m^{-3}$ in NO_3-OA1 and 3.1 $\mu g\,m^{-3}$ in NO_3-OA2 and 53 % in NO_3-OA1 and 34 % in NO_3-OA2, respectively. These proportions were lower than the corresponding proportions of NO_3-OA in New York City (74 %) (Sun et al., 2012b) and Windsor (78 %) (McGuire et al., 2014). The nitrate in NO_3-OA1 and NO_3-OA2 accounted for 88 % of the total nitrate measured in this study. The mass spectra of the two NO_3-OA factors showed peaks at m/z 16, 17, 30 and 46 (Fig. 3a). However, the contribution of $C_xH_yO_z$ fragments, especially CO_2^{+} (m/z 44), to the mass spectrum of NO_3-OA2 was slightly higher (12.2 %) than in the mass spectrum of NO_3-OA1. This value also represented the second highest CO_2^{+} of all the factors from the PMF analysis (Fig. 3a). The significant contribution of $C_xH_yO_z$ fragments implies that

ACPD
15, 18537–18576, 2015

this factor had a greater age than NO_3-OA1. Accordingly, the difference in oxidation could also be obtained from the O/C ratios, which were clearly higher for NO_3-OA2 (0.61) than for NO_3-OA1 (0.35).

Of all the factors, the two NO_3-OA factors contributed the most to the NR-PM_1 mass (42 %); the contributions of NO_3-OA1 and NO_3-OA2 were 28 and 14 %, respectively (Fig. 4c). The total contribution proportion is consistent with that observed in Windsor (45 %), where the NO_3-OA factor also contributed the most to the submicron PM mass (McGuire et al., 2014). The diurnal cycle of NO_3-OA1 showed elevated concentrations in the early morning when the air temperature was low and the RH was high (Fig. 5a). The NO_3-OA1 concentration decreased rapidly during the daytime and showed a minimum in the late afternoon (12.3 $\mu g\,m^{-3}$). Such diurnal variation was consistent with the diurnal profile of the equilibrium constant (Kp) of $NH_3(g) + HNO_3(g) \rightarrow NH_4NO_3(s)$, indicating that the partitioning between particle-phase nitrate and gas-phase HNO_3 might have played a major role. This diurnal profile is very close to the results reported for NO_3-OA by Sun et al. (2012b). However, NO_3-OA2 presented a markedly low mass concentration value at 11:00 (3.6 $\mu g\,m^{-3}$), which then increased until 18:00, consistent with the diurnal profile of the photochemical production of nitrate. The peak value was evident at 18:00 (approximately 9.2 $\mu g\,m^{-3}$; Fig. 5b), which illustrates a dominant source of nitrate from photochemical production for NO_3-OA2. These results suggest that a PMF analysis of the combined organic and inorganic aerosols is able to identify the two different formation mechanisms of nitrate, i.e., heterogeneous hydrolysis of N_2O_5 and photochemical production, both of which play important roles in nitrate formation. There was a strong correlation between nitrate and NO_3-OA1 (R^2 = 0.82) compare to nitrate and NO_3-OA2 (R^2 = 0.59) (Fig. S8a and b), suggesting that heterogeneous hydrolysis of N_2O_5 played a more important role than photochemical processes in the formation of nitrate during winter in 2014. This conclusion is supported by the contributions of the two NO_3-OA factors mentioned above (28 and 14 % for NO_3-OA1 and NO_3-OA2, respectively) and by the results of Zhao et al. (2013) and Zheng et al. (2014b) for winter in Beijing. By analyzing the sulfate, nitrate and ammonium con-

ACPD
15, 18537–18576, 2015

tents in $PM_{2.5}$ in four cities in China, Pathak et al. (2009) suggested that nitrate was usually formed through heterogeneous hydrolysis of N_2O_5 on the surfaces of moist and acidic aerosols in Beijing and Shanghai, especially during humid and hazy weather.

The ratio of NH_4^+/SO_4^{2-} has been used to judge the major nitrate formation in different seasons. When the ratio was > 1.5, the aerosols were identified as ammonium rich (AR) (or ammonium poor (AP) when the ratio was < 1.5) (Pathak, 2004; Pathak et al., 2004). After two years of online observations in Hong Kong, Griffith et al. (2015) found that the vast majority of winter nitrate data were associated with AR aerosols ($NH_4^+/SO_4^{2-} > 1.5$), with the mass concentration peak at night. However, the summer nitrate data were in an AP regime, showing peaks in the daytime centered around solar noon during the summer, which tracked the concentrations of nitric acid, a photochemical tracer. The ratio NH_4^+/SO_4^{2-} was also calculated in January 2014, with an average of 3.2 ± 1.3. More than 83 % of the nitrate data was associated with AR aerosols corresponding to a higher NR-PM_1 level. This is consistent with the domination of NO_3-OA1 in this campaign.

The relationship between the two NO_3-OA factors and relative humidity (RH) can also be used to demonstrate the differences in their formation mechanisms. Figure 4d presents the variations in the two NO_3-OA factors and the SO_4-OA factor with the increase in RH observed in this study. The variations of the two NO_3-OA factors can be divided into three sections: (1) in which they showed a remarkably similar increase when RH < 30 %, (2) in which the increase rate of NO_3-OA2 was distinctly lower than that of NO_3-OA1 in an RH range of 30 to 50 %, and (3) in which the two NO_3-OA factors presented opposite trends when RH > 50 %, i.e., NO_3-OA1 maintained an increasing trend with a rate even higher than that of SO_4-OA, whereas NO_3-OA2 decreased almost linearly. The observed reduction at RH > 80 % may be due to a larger expected range of particle diameters for the OA factors with a strong hygroscopicity at high RH. As a result, a considerable fraction of NO_3-OA factors might be located in particles with diameters between 1 and 2.5 $\mu g\,m^{-3}$ that AMS cannot detect. It is clear that RH = 50 % represents a threshold value for differences in trends between the NO_3-OA1 and NO_3-

ACPD
15, 18537–18576, 2015

OA2 factors. This is in agreement with the results of Sun et al. (2013a) based on the Extend Aerosol Thermodynamics Model (E-AIM, Model II) during winter in Beijing. After combining the E-AIM with aerosol chemical composition data, they found that RH ≤ 50 % (or > 50 %) is the threshold liquid water content (LWC). They also showed a substantial increase of LWC with increasing RH observed at RH > 50 %, indicating the importance of aerosol water at elevated RH levels. This diversity of variation of NO_3-OA1 and NO_3-OA2 with RH supports the different formation pathways suggested by the results of the present study.

In addition to formation through different mechanisms, part of NO_3-OA1 could be oxidized to NO_3-OA2 in daytime as a result of increasing temperature. Therefore, these two NO_3-OA factors represent not only two formation mechanisms of nitrate but also an aging process of general NO_3-OA factors in the atmosphere.

Very similar factors were also obtained in winter 2013 by Sun et al. (2014), and three SOA (secondary OA) factors were identified in their study, two of which were identified as SV-OOA and LSOA (local SOA) and showed very similar characteristics to NO_3-OA1 and NO_3-OA2 in our study, respectively. This indicates that the formation mechanisms of SOA in winter in Beijing have been consistent in recent years.

The SO_4-OA factor was also identified by Sun et al. (2012b) and McGuire et al. (2014). This factor was primarily composed of ammonium sulfate (9.8 $\mu g\,m^{-3}$), which accounted for 67 % of its total mass (Fig. 4a and b). Similar to a previously published mass spectrum of atomized $(NH_4)_2SO_4$ (Hogrefe et al., 2004), SO_4-OA in the present study also exhibited major peaks at m/z 16, 17, 48, 64, 80 and 81 (Fig. 3a). The SO_4-OA factor showed close correlation with sulfate ($R^2 = 0.89$) and the oxygenated ion CO_2^+ (m/z 44, $R^2 = 0.71$; Fig. S8c). Note that 30 % of the mass of this factor was classified as organic with a high degree of oxidation (O/C = 0.89). The organic components contained in this factor were the most oxidized of the six factors identified in this study (Fig. 3a), consistent with reports for the SO_4-OA factor in New York City and Windsor (Sun et al., 2012b; McGuire et al., 2014). The SO_4-OA factor on average contributed 27 % to the NR-PM_1 mass concentration (Fig. 4c). The correlation

ACPD
15, 18537–18576, 2015

of SO_4-OA with SO_2 was moderate (R^2 = 0.31), implying that this factor was likely influenced by both long-range transport and local sources. The diurnal profile of SO_4-OA was very similar to that of sulfate (Fig. 5c), suggesting that SO_4-OA was a highly aged secondary factor. Indeed, sulfate in the SO_4-OA factor contributed 83 % of the total sulfate mass. Similar to the result in New York City, there was almost no nitrate contained in the SO_4-OA factor, which can be attributed to the differences in the formation mechanisms and the volatility between them (Sun et al., 2012b).

3.2.2 COA and HOA

COA and HOA are typical primary OA components that have been identified in Beijing and other sites. COA and HOA showed mass spectral profiles resembling those from cooking emissions and gasoline and diesel combustion (Mohr et al., 2009; Allan et al., 2010; Schneider et al., 2006). They had low O/C ratios of 0.08 and 0.12 and were primarily dominated by the ion series of $C_nH^+_{2n+1}$ and $C_nH^+_{2n-1}$ (Fig. 3a). The most noticeable difference between COA and HOA are their diurnal profiles. COA showed three peaks: in the morning (06:00–07:00), at noon (12:00–14:00) and in the evening (19:00–24:00) (Fig. 5d). The peaks in the morning and at noon corresponded to breakfast and lunch times, while the lowering of the mixed layer height would have been a very important factor for the stronger and longer peak in the evening. HOA were consistent with the emissions from traffic exhaust, which showed a pronounced morning peak associated with traffic emissions, the highest concentration at 23:00 and the lowest concentration at 14:00 (Fig. 5e). The corresponding mass concentrations were 5.9 and 3.0 $\mu g\,m^{-3}$, respectively.

There was a significant correlation between COA and a number of $C_xH_yO^+_1$ ions including $C_6H_{10}O^+$ (R^2 = 0.82, Fig. S8d), which represented prominent peaks in the source spectra of cooking emissions. These ions could be used as spectral markers for COA (Sun et al., 2011). HOA correlated well with combustion tracers such as NO_x (R^2 = 0.65) and BC (R^2 = 0.64), and the correlation coefficient R^2 of HOA and $C_3H^+_7$,

ACPD
15, 18537–18576, 2015

a typical ion of $C_nH^+_{2n+1}$, was approximately 0.73 (Fig. S8e). In addition, COA and HOA showed a similar contribution to NR-PM_1 (8 and 9 %, respectively).

Note that the two primary factors (COA and HOA) contained little inorganic ammonium sulfate or ammonium nitrate and were almost completely organic (> 96 %) (Fig. 4b). This can be considered evidence for the existence of various different sources of primary organic particles and secondary inorganic species. A higher contribution of organics (> 97 %) was also found by Sun et al. (2012b).

3.2.3 CCOA

The final factor identified through the PMF analysis was CCOA, which was also reported in winter 2012 and 2013 in Beijing and other studies worldwide (Sun et al., 2013b; Zhang et al., 2014; Wang et al., 2013; Dall'Osto et al., 2013). The mass spectrum of CCOA was dominated by alkyl fragments ($C_nH^+_{2n+1}$ and $C_nH^+_{2n-1}$), which is typical of primary organic aerosols derived from fossil fuel combustion. When the inorganic species were combined, the contribution of m/z 36 (HCl^+; 13.1 %) was the highest ion in the mass spectrum. The contributions of m/z 16 (NH^+_2), m/z 17 (NH^+_3), m/z 30 (NO^+), m/z 35 (Cl^+) and m/z 46 (NO^+_2) should also not be neglected (Fig. 3a). These mass characteristics are very similar to the chloride factor in Windsor (McGuire et al., 2014).

The chloride in CCOA accounted for 61 % of the total chloride in NR-PM_1 (Fig. 4b). The O/C ratio for CCOA was 0.22, which was higher than the ratios for COA (0.08) and HOA (0.12). This suggests that CCOA was more aged than the typical primary OA factors. Similar to previous results from winter in Beijing (Sun et al., 2013b; Zhang et al., 2014), there was a temporal trend in the CCOA data that was comparable to the time series for chloride (R^2 = 0.71; Fig. S8f). In addition, the average CCOA fraction of the total NR-PM_1 was approximately 14 % (Fig. 4c).

It is important to note that when the organic and inorganic HR spectral matrices were integrated into one unified dataset for PMF analysis, the inorganic species were apportioned into several OA factors because of their different formation mechanisms

ACPD
15, 18537–18576, 2015

and evolution processes. These results could provide more information regarding the sources, evolution and oxidation of different factors, which may be particularly useful in understanding the inorganic species present in particles (~ 50 % of NR-PM_1).

3.3 Evolution of OA

The PMF analysis (Sect. 3.2) showed the six factors originating from diverse sources, including both direct emissions and generation through a variety of chemical reactions in the atmosphere. This observed complexity poses a challenge to our ability to explicitly characterize the chemical composition of these components. Therefore, it is important to investigate the evolution of these factors in the atmosphere. In this section, the well-known methods of the triangle plot (f_{44} vs. f_{43}) (Ng et al., 2010) and the Van Krevelen diagram (Heald et al., 2010) are used to analyze this critical problem. Figure 6a shows that the HOA and COA both exhibit low oxidative properties with varying f_{43}, which are located at the bottom of the triangular region. The CCOA and NO_3-OA1 are slightly higher due to these factors exercising a certain degree of oxidation, with f_{44} of 0.02 and 0.03, respectively (Fig. 6a). During the aging process, OA evolves to the upper corner, followed by a decrease in f_{43} and a significant increase in f_{44}, with a value higher than 0.1. The SO_4-OA factor subsequently shows a state of high oxidation, and f_{44} is higher than 0.15 (Fig. 6a). These variation trends are very close to the results for New York City (Sun et al., 2012b), although the factors identified by PMF are not identical to ours.

Because the triangle plot represents an integration of OOA factors in which m/z 44 is primarily CO_2^+ and m/z 43 is primarily $C_2H_3O^+$, we also examined the relationship between $f_{CO_2^+}$ (fraction of CO_2^+ in OA) and $f_{C_2H_3O^+}$ (fraction of $C_2H_3O^+$ in OA) in Fig. 6b. The OA factors exhibit different behaviors for $f_{CO_2^+}$ vs. $f_{C_2H_3O^+}$. The POA factors of HOA and COA are located in the bottom-left corner, with the lowest $f_{CO_2^+}$ and $f_{C_2H_3O^+}$. The $f_{CO_2^+}$ and $f_{C_2H_3O^+}$ for CCOA are only slightly higher than for HOA and COA, which is similar to the trend of f_{44} vs. f_{43}. In addition, NO_3-OA1 and NO_3-OA2 are located

ACPD
15, 18537–18576, 2015

at different sites in the triangular region; NO_3-OA2 has a higher $f_{CO_2^+}$ than NO_3-OA1, indicating their different sources and properties. The aging of OA can therefore be characterized by two stages: (1) the initial oxidization of fresh OA, such as HOA/COA, appears to involve a synchronous increase in both $f_{CO_2^+}$ and $f_{C_2H_3O^+}$ and evolves into the triangular region first, (2) the further oxidation of less-oxidized OA (such as NO_3-OA1) subsequently follows a pathway involving a decrease in $f_{C_2H_3O^+}$ and an increase in $f_{CO_2^+}$. These two evolving pathways are in agreement with the evolution of H/C vs. O/C shown in the Van Krevelen diagram (Fig. 6c). The initial oxidation of POA shows a steeper slope than −1, which is probably driven by the functionalization via incorporation of carbonyl groups (Ng et al., 2011). Freshly formed SOA (represented by NO_3-OA1) evolves in different ways, with a shallower slope of ∼ 0.5.

3.4 Comparison of heavy pollution periods in January 2013 and 2014

Four heavy pollution events were selected to compare the variations in pollution characteristics between January 2013 and 2014. These pollution periods are marked in grey in Fig. 1 (P1 and P2 occurred in 2013, and P3 and P4 occurred in 2014) and represent the most polluted processes for the two campaigns. There was a significant decrease in the NR-PM_1 average mass concentration during the pollution events that occurred in January 2014 (Fig. 7). The corresponding NR-PM_1 mass concentrations of P3 and P4 were only 75.6 and 61.1 $\mu g\,m^{-3}$, respectively, which were far below the concentrations observed during P1 (117.0 $\mu g\,m^{-3}$) and P2 (210.2 $\mu g\,m^{-3}$). The composition of NR-PM_1 also showed clear differences between the 2013 and 2014 heavy pollution periods. In January 2013, the contributions of organics were 44 and 41 % for P1 and P2, respectively, while in January 2014, they increased to 50 and 45 % for P3 and P4, respectively. This may have been caused by the decrease in NR-PM_1 in January 2014 (discussed in Sect. 3.1).

In addition to the difference in the contributions of organics, the composition of inorganic species also showed some interesting variations. In January 2013, the inorganic

ACPD
15, 18537–18576, 2015

species were always dominated by sulfate; the contributions of sulfate for P1 and P2 were 27 and 28 %, respectively, which were clearly higher than for other inorganic species. Conversely, the dominance of sulfate was no longer apparent in 2014; there was a significant reduction in the contribution of sulfate but an increase in that of nitrate. In P4, the contribution of nitrate (20 %) was even slightly higher than that of sulfate (19 %, Fig. 7). In general, these differences in the mass concentration of NR-PM_1 and its composition may have been caused by variations in the sources and meteorological factors between January 2013 and January 2014. It is difficult to discuss changes in the sources for two reasons: (1) a detailed discussion would require extensive and timely survey data, which are very difficult to obtain, and (2) it is unlikely that the annual average emissions of primary pollutants would present significant changes during such a short period of time (one or two years) due to the general stability of the urban infrastructure, as demonstrated by Zheng et al. (2014b). They found that annual average emissions of primary $PM_{2.5}$, SO_2 and NO_x showed only slight differences between 2013 and 2012 (1.2, −1.3 and 0.8 %, respectively) in the Beijing–Tianjin–Hebei region. However, differences caused by unfavorable meteorology could result in a significant increase in $PM_{2.5}$ over the North China Plain (Zheng et al., 2014b). Therefore, meteorological parameters were the key factors influencing the formation of haze because they affected the horizontal transport, vertical mixing, atmospheric reaction rates and scavenging of air pollutants. We therefore focused only on the variations of meteorological factors between January 2013 and 2014 in this study. These analyses also represent a wealth of useful information regarding the changes in the pollution characteristics.

The average temperature (±1 SD) in January 2014 was 1.5 ± 3.4 °C, which is higher than the observation of −2.8 ± 3.1 °C in January 2013 (Fig. S9). Figure 8a shows the statistical results of the probability of temperature. It is clear that the temperature in January 2013 was typically distributed between −5 and 0 °C (probability = 64 %), while the temperature in January 2014 was mainly distributed between 0 and 5 °C (probability = 48 %). Significant differences in temperature between the four events can also

ACPD
15, 18537–18576, 2015

be clearly observed in Fig. 9a. The elevated temperature was more conducive to the generation of nitrate rather than sulfate through daytime photochemical production.

Relative humidity affects aerosol formation in a number of ways, e.g., aqueous-phase reactions and gas-particle partitioning (Altieri et al., 2008; Hennigan et al., 2008). The average RH, however, decreased from 49 % in January 2013 to 34 % in 2014. Compared with the statistical results of RH for January 2013, the RH in January 2014 was primarily below 40 % (probability = 73 %, Fig. 8b). Figure 9b presents the diurnal profiles of RH for the four heavy pollution events. The RH for P3 and P4 were significantly lower than that for P1 and P2; in particular, the RH throughout the full daily cycle for P2 was 70 % higher. Many previous studies have concluded that the aqueous-phase reaction during fog processes is a very important pathway for the generation of inorganic species in winter in Beijing (Sun et al., 2013a; Zhang et al., 2014; Huang et al., 2014). This aqueous-phase effect is much stronger for sulfate than for nitrate; there is weaker aqueous-phase production associated with lower nitrogen oxidation ratios (Sun et al., 2014). Sun et al. (2013a) found that fog processing of SO_2 could contribute to ~ 70 % of sulfate production; whereas, aqueous-phase production accounts for < 30 % of nitrate production. Huang et al. (2014) found the largest increase in sulfate (almost five-fold) alongside an RH increase from 37.4 to 77.5 %; nevertheless, nitrate and ammonium only increased by a factor of two or three. They believed that the faster SO_2 oxidation rate in the aqueous phase was a critical factor in the larger increase in sulfate than nitrate. Therefore, the decrease in RH in January 2014 compared to that in 2013 was a critical factor in the changes in the contribution of inorganic species in our study, especially for sulfate and nitrate. Compared to the temperature and RH, air pressure and wind speed have no regular difference between pollution events (Fig. 9c and d). This implies that these two parameters are not key factors in explaining the difference in heavy pollution events in the two January periods.

Regional transport has been identified as an important contributor to the PM pollution in Beijing (Jia et al., 2008; Zheng et al., 2014b; Sun et al., 2014; Wang et al., 2014b). Sun et al. (2014) found that the regional transport contributed 66 % on aver-

ACPD
15, 18537–18576, 2015

age to PM_1 during a heavy pollution event in winter in 2013. The impacts of various source regions on the PM pollution in January 2013 and January 2014 in Beijing were explored using the hybrid single-particle Lagrangian integrated trajectory (HYSPLIT) model. The analysis steps were as follows. First, 48 h back trajectories (BTs) starting at 200 m a.g.l. in Beijing (39.97°, 116.37°) were calculated every 6 h (at 00:00, 06:00, 12:00 and 18:00 LT) throughout the two campaigns. The trajectories were then clustered according to their similarity in a spatial distribution using the software HYSPLIT4. As a result, five-cluster and four-cluster solutions were adopted for the January 2013 and January 2014 campaigns, respectively (Fig. 8c and d).

The air masses in the two campaigns were remarkably similar; almost all air masses originated from western China (originating from 180–360° N). The air masses that originated from the direction between south and west (180–270° N) belong to the pollution air mass because there are a large number of polluting industries, such as power plants, steel mills, cement mills and the petrochemical industry, in this area. However, the air masses that originated from the direction between west and north (270–360° N) belonged to the clean air mass because there are almost no pollution sources in this area. Figure 8c and d shows that, although the directions of the air masses in January 2013 and 2014 were not perfectly consistent, the NR-PM_1 mass concentration of each cluster in January 2014 was significantly lower than the NR-PM_1 mass concentration in the cluster in January 2013 that corresponded to the close direction. The NR-PM_1 mass concentration in the most polluted cluster (cluster 5 and 4 in January 2013 and 2014, respectively), for example, decreased from 123 to 87.9 $\mu g\,m^{-3}$, and the NR-PM_1 mass concentration in the cleanest cluster (cluster 1 in January 2013 and 2014) also decreased by 5.1 $\mu g\,m^{-3}$. Therefore, the reduction of regional transport is another important reason for the lower NR-PM_1 mass concentration in January 2014.

According to the above discussion, the NR-PM_1 mass concentration in Beijing can be attributed to local emissions and regional transport. Therefore, the most effective way to control fine particle pollution is joint prevention and control at the regional level, rather than focusing on an individual city, especially in the case of severe haze events.

ACPD
15, 18537–18576, 2015

4 Conclusions

In this study, non-refractory submicron aerosol particles in Beijing were measured in situ using a high-resolution time-of-flight aerosol mass spectrometer during January 2014 in an intensive field study. The first aim was to compare the results between the same periods in January 2013 and 2014 because the city experienced its most serious PM pollution of this century in January 2013. The comparison showed that NR-PM_1 pollution was weaker in January 2014; the reduced amplitude of the NR-PM_1 mass concentration was approximately 40 $\mu g\,m^{-3}$, which was primarily caused by variations in meteorological conditions. There was also a significant change in the composition of NR-PM_1 during the heavy pollution events of January 2014, with a greater contribution from nitrate specifically.

We first merged high-resolution mass spectra of organic and inorganic aerosols from AMS measurements and then applied PMF to the combined mass spectral matrix to investigate the sources and evolution processes of submicron aerosols in January 2014 in Beijing. Six factors were identified. The NO_3-OA1 and NO_3-OA2 factors corresponded to two major formation mechanisms of nitrate, showed different degrees of oxidation, and contributed most to the NR-PM_1 mass (42 %). The SO_4-OA factor showed the highest degree of oxidation (O/C = 0.89) of all OA factors. The HOA and COA factors contained negligible amounts of inorganic species. CCOA was mainly emitted from coal combustion in the city, which contained a high contribution from chloride in the mass spectrum. The triangle plot (f_{44} vs. f_{43}) and Van Krevelen diagram methods were combined to analyze the evolution of the factors. We found that the initial oxidation of POA was likely driven by functionalization via incorporation of carbonyl groups; however, the transition from less-oxidized to more-oxidized OOA most likely originated from the addition of both acid and alcohol functional groups with little fragmentation. The comparison of several heavy pollution events during the two campaigns indicates that higher temperature, lower RH and reduced transport from surrounding areas can explain the differences in NR-PM_1 mass concentration and composition be-

ACPD
15, 18537–18576, 2015

tween the two January studies. Consequently, the most effective way to control fine particle pollution is joint prevention and control at the regional level, rather than a focus on an individual city.

The Supplement related to this article is available online at doi:10.5194/acpd-15-18537-2015-supplement.

Acknowledgements. This study was supported by the "Strategic Priority Research Program" of the Chinese Academy of Sciences (XDA05100100 & XDB05020000) and the National Natural Science Foundation of China (NO.41 230 642, 41 175 107 and 41 275 139). We gratefully acknowledge these financial supports.

References

Aiken, A. C., DeCarlo, P. F., Kroll, J. H., Worsnop, D. R., Huffman, J. A., Docherty, K. S., Ulbrich, I. M., Mohr, C., Kimmel, J. R., Sueper, D., Sun, Y., Zhang, Q., Trimborn, A., Northway, M., Ziemann, P. J., Canagaratna, M. R., Onasch, T. B., Alfarra, M. R., Prevot, A. S. H., Dommen, J., Duplissy, J., Metzger, A., Baltensperger, U., and Jimenez, J. L.: O/C and OM/OC ratios of primary, secondary, and ambient organic aerosols with high-resolution time-of-flight aerosol mass spectrometry, Environ. Sci. Technol., 42, 4478–4485, 2008.

Allan, J. D., Jimenez, J. L., Williams, P. I., Alfarra, M. R., Bower, K. N., Jayne, J. T., Coe, H., and Worsnop, D. R.: Quantitative sampling using an Aerodyne aerosol mass spectrometer, 1. Techniques of data interpretation and error analysis, J. Geophys. Res., 108, 4090, doi:10.1029/2002jd002358, 2003.

Allan, J. D., Williams, P. I., Morgan, W. T., Martin, C. L., Flynn, M. J., Lee, J., Nemitz, E., Phillips, G. J., Gallagher, M. W., and Coe, H.: Contributions from transport, solid fuel burning and cooking to primary organic aerosols in two UK cities, Atmos. Chem. Phys., 10, 647–668, doi:10.5194/acp-10-647-2010, 2010.

Altieri, K. E., Seitzinger, S. P., Carlton, A. G., Turpin, B. J., Klein, G. C., and Marshall, A. G.: Oligomers formed through in-cloud methylglyoxal reactions: chemical composition, proper-

ACPD
15, 18537–18576, 2015

ties, and mechanisms investigated by ultra-high resolution FT-ICR mass spectrometry, Atmos. Environ., 42, 1476–1490, doi:10.1016/j.atmosenv.2007.11.015, 2008.
Canagaratna, M. R., Jayne, J. T., Jimenez, J. L., Allan, J. D., Alfarra, M. R., Zhang, Q., Onasch, T. B., Drewnick, F., Coe, H., Middlebrook, A., Delia, A., Williams, L. R., Trimborn, A. M., Northway, M. J., DeCarlo, P. F., Kolb, C. E., Davidovits, P., and Worsnop, D. R.: Chemical and microphysical characterization of ambient aerosols with the aerodyne aerosol mass spectrometer, Mass Spectrom. Rev., 26, 185–222, doi:10.1002/mas.20115, 2007.
Charlson, R. J., Schwartz, S. E., Hales, J. M., Cess, R. D., Coakley, J. A., Hansen, J. E., and Hofmann, D. J.: Climate forcing by anthropogenic aerosols, Science, 255, 423–430, doi:10.1126/science.255.5043.423, 1992.
Chow, J. C., Watson, J. G., Mauderly, J. L., Costa, D. L., Wyzga, R. E., Vedal, S., Hidy, G. M., Altshuler, S. L., Marrack, D., Heuss, J. M., Wolff, G. T., Pope, C. A., and Dockery, D. W.: Health effects of fine particulate air pollution: lines that connect, JAPCA J. Air Waste Ma., 56, 1368–1380, 2006.
Crippa, M., El Haddad, I., Slowik, J. G., DeCarlo, P. F., Mohr, C., Heringa, M. F., Chirico, R., Marchand, N., Sciare, J., Baltensperger, U., and Prévôt, A. S. H.: Identification of marine and continental aerosol sources in Paris using high resolution aerosol mass spectrometry, J. Geophys. Res.-Atmos., 118, 1950–1963, doi:10.1002/jgrd.50151, 2013.
Dall'Osto, M., Ovadnevaite, J., Ceburnis, D., Martin, D., Healy, R. M., O'Connor, I. P., Kourtchev, I., Sodeau, J. R., Wenger, J. C., and O'Dowd, C.: Characterization of urban aerosol in Cork city (Ireland) using aerosol mass spectrometry, Atmos. Chem. Phys., 13, 4997–5015, doi:10.5194/acp-13-4997-2013, 2013.
DeCarlo, P. F., Kimmel, J. R., Trimborn, A., Northway, M. J., Jayne, J. T., Aiken, A. C., Gonin, M., Fuhrer, K., Horvath, T., Docherty, K. S., Worsnop, D. R., and Jimenez, J. L.: Field-deployable, high-resolution, time-of-flight aerosol mass spectrometer, Anal. Chem., 78, 8281–8289, doi:10.1029/, 2006.
Drewnick, F., Hings, S. S., DeCarlo, P., Jayne, J. T., Gonin, M., Fuhrer, K., Weimer, S., Jimenez, J. L., Demerjian, K. L., Borrmann, S., and Worsnop, D. R.: A new Time-of-Flight Aerosol Mass Spectrometer (TOF-AMS) – instrument description and first field deployment, Aerosol Sci. Tech., 39, 637–658, doi:10.1080/02786820500182040, 2005.
Griffith, S. M., Huang, X. H. H., Louie, P. K. K., and Yu, J. Z.: Characterizing the thermodynamic and chemical composition factors controlling $PM_{2.5}$ nitrate: insights gained from two years of

ACPD
15, 18537–18576, 2015

online measurements in Hong Kong, Atmos. Environ., doi:10.1016/j.atmosenv.2015.02.009, in press, 2015.
He, L.-Y., Huang, X.-F., Xue, L., Hu, M., Lin, Y., Zheng, J., Zhang, R., and Zhang, Y.-H.: Submicron aerosol analysis and organic source apportionment in an urban atmosphere in Pearl River Delta of China using high-resolution aerosol mass spectrometry, J. Geophys. Res., 116, D12304, doi:10.1029/2010jd014566, 2011.
Heald, C. L., Kroll, J. H., Jimenez, J. L., Docherty, K. S., DeCarlo, P. F., Aiken, A. C., Chen, Q., Martin, S. T., Farmer, D. K., and Artaxo, P.: A simplified description of the evolution of organic aerosol composition in the atmosphere, Geophys. Res. Lett., 37, L08803, doi:10.1029/2010gl042737, 2010.
Hennigan, C. J., Bergin, M. H., Dibb, J. E., and Weber, R. J.: Enhanced secondary organic aerosol formation due to water uptake by fine particles, Geophys. Res. Lett., 35, L18801, doi:10.1029/2008gl035046, 2008.
Hogrefe, O., Drewnick, F., Lala, G. G., Schwab, J. J., and Demerjian, K. L.: Development, operation and applications of an aerosol generation, calibration and research facility, Aerosol Sci. Tech., 38, 196–214, doi:10.1080/02786820390229516, 2004.
Huang, K., Zhuang, G., Wang, Q., Fu, J. S., Lin, Y., Liu, T., Han, L., and Deng, C.: Extreme haze pollution in Beijing during January 2013: chemical characteristics, formation mechanism and role of fog processing, Atmos. Chem. Phys. Discuss., 14, 7517–7556, doi:10.5194/acpd-14-7517-2014, 2014.
Huang, X.-F., He, L.-Y., Hu, M., Canagaratna, M. R., Sun, Y., Zhang, Q., Zhu, T., Xue, L., Zeng, L.-W., Liu, X.-G., Zhang, Y.-H., Jayne, J. T., Ng, N. L., and Worsnop, D. R.: Highly time-resolved chemical characterization of atmospheric submicron particles during 2008 Beijing Olympic Games using an Aerodyne High-Resolution Aerosol Mass Spectrometer, Atmos. Chem. Phys., 10, 8933–8945, doi:10.5194/acp-10-8933-2010, 2010.
Huang, X.-F., He, L.-Y., Hu, M., Canagaratna, M. R., Kroll, J. H., Ng, N. L., Zhang, Y.-H., Lin, Y., Xue, L., Sun, T.-L., Liu, X.-G., Shao, M., Jayne, J. T., and Worsnop, D. R.: Characterization of submicron aerosols at a rural site in Pearl River Delta of China using an Aerodyne High-Resolution Aerosol Mass Spectrometer, Atmos. Chem. Phys., 11, 1865–1877, doi:10.5194/acp-11-1865-2011, 2011.
IPCC: Climate Change 2013: The Physical Science Basis, Intergovernmental Panel on Climate Change, Cambridge University Press, New York, 571–740, 2013.

ACPD
15, 18537–18576, 2015

Jayne, J. T., Leard, D. C., Zhang, X., Davidovits, P., Smith, K. A., Kolb, C. E., and Worsnop, D. R.: Development of an aerosol mass spectrometer for size and composition analysis of submicron particles, Aerosol Sci. Tech., 33, 49–70, doi:10.1080/027868200410840, 2000.

Ji, D., Wang, Y., Wang, L., Chen, L., Hu, B., Tang, G., Xin, J., Song, T., Wen, T., Sun, Y., Pan, Y., and Liu, Z.: Analysis of heavy pollution episodes in selected cities of northern China, Atmos. Environ., 50, 338–348, doi:10.1016/j.atmosenv.2011.11.053, 2012.

Jia, Y., Rahn, K. A., He, K., Wen, T., and Wang, Y.: A novel technique for quantifying the regional component of urban aerosol solely from its sawtooth cycles, J. Geophys. Res., 113, D21309, doi:10.1029/2008jd010389, 2008.

Jimenez, J. L., Jayne, J. T., Shi, Q., Kolb, C. E., Worsnop, D., and Yourshaw, I.: Ambient aerosol sampling using the Aerodyne Aerosol Mass Spectrometer, J. Geophys. Res., 108, doi:10.1029/2001jd001213, 2003.

Jimenez, J. L., Canagaratna, M. R., Donahue, N. M., Prevot, A. S., Zhang, Q., Kroll, J. H., DeCarlo, P. F., Allan, J. D., Coe, H., Ng, N. L., Aiken, A. C., Docherty, K. S., Ulbrich, I. M., Grieshop, A. P., Robinson, A. L., Duplissy, J., Smith, J. D., Wilson, K. R., Lanz, V. A., Hueglin, C., Sun, Y. L., Tian, J., Laaksonen, A., Raatikainen, T., Rautiainen, J., Vaattovaara, P., Ehn, M., Kulmala, M., Tomlinson, J. M., Collins, D. R., Cubison, M. J., Dunlea, E. J., Huffman, J. A., Onasch, T. B., Alfarra, M. R., Williams, P. I., Bower, K., Kondo, Y., Schneider, J., Drewnick, F., Borrmann, S., Weimer, S., Demerjian, K., Salcedo, D., Cottrell, L., Griffin, R., Takami, A., Miyoshi, T., Hatakeyama, S., Shimono, A., Sun, J. Y., Zhang, Y. M., Dzepina, K., Kimmel, J. R., Sueper, D., Jayne, J. T., Herndon, S. C., Trimborn, A. M., Williams, L. R., Wood, E. C., Middlebrook, A. M., Kolb, C. E., Baltensperger, U., and Worsnop, D. R.: Evolution of organic aerosols in the atmosphere, Science, 326, 1525–1529, doi:10.1126/science.1180353, 2009.

Liu, X. G., Li, J., Qu, Y., Han, T., Hou, L., Gu, J., Chen, C., Yang, Y., Liu, X., Yang, T., Zhang, Y., Tian, H., and Hu, M.: Formation and evolution mechanism of regional haze: a case study in the megacity Beijing, China, Atmos. Chem. Phys., 13, 4501–4514, doi:10.5194/acp-13-4501-2013, 2013.

McGuire, M. L., Chang, R. Y.-W., Slowik, J. G., Jeong, C.-H., Healy, R. M., Lu, G., Mihele, C., Abbatt, J. P. D., Brook, J. R., and Evans, G. J.: Enhancing non-refractory aerosol apportionment from an urban industrial site through receptor modeling of complete high time-resolution aerosol mass spectra, Atmos. Chem. Phys., 14, 8017–8042, doi:10.5194/acp-14-8017-2014, 2014.

ACPD
15, 18537–18576, 2015

Middlebrook, A. M., Bahreini, R., Jimenez, J. L., and Canagaratna, M. R.: Evaluation of composition-dependent collection efficiencies for the aerodyne aerosol mass spectrometer using field data, Aerosol Sci. Tech., 46, 258–271, doi:10.1080/02786826.2011.620041, 2012.

Mohr, C., Huffman, J. A., Cubison, M. J., Aiken, A. C., Docherty, K. S., Kimmel, J. R., Ulbrich, I. M., Hannigan, M., and Jimenez, J. L.: Characterization of primary organic aerosol emissions from meat cooking, trash burning, and motor vehicles with high-resolution aerosol mass spectrometry and comparison with ambient and chamber observations, Environ. Sci. Technol., 43, 2443–2449, doi:10.1021/es8011518, 2009.

Mohr, C., DeCarlo, P. F., Heringa, M. F., Chirico, R., Slowik, J. G., Richter, R., Reche, C., Alastuey, A., Querol, X., Seco, R., Peñuelas, J., Jiménez, J. L., Crippa, M., Zimmermann, R., Baltensperger, U., and Prévôt, A. S. H.: Identification and quantification of organic aerosol from cooking and other sources in Barcelona using aerosol mass spectrometer data, Atmos. Chem. Phys., 12, 1649–1665, doi:10.5194/acp-12-1649-2012, 2012.

Ng, N. L., Canagaratna, M. R., Zhang, Q., Jimenez, J. L., Tian, J., Ulbrich, I. M., Kroll, J. H., Docherty, K. S., Chhabra, P. S., Bahreini, R., Murphy, S. M., Seinfeld, J. H., Hildebrandt, L., Donahue, N. M., DeCarlo, P. F., Lanz, V. A., Prévôt, A. S. H., Dinar, E., Rudich, Y., and Worsnop, D. R.: Organic aerosol components observed in Northern Hemispheric datasets from Aerosol Mass Spectrometry, Atmos. Chem. Phys., 10, 4625–4641, doi:10.5194/acp-10-4625-2010, 2010.

Ng, N. L., Canagaratna, M. R., Jimenez, J. L., Chhabra, P. S., Seinfeld, J. H., and Worsnop, D. R.: Changes in organic aerosol composition with aging inferred from aerosol mass spectra, Atmos. Chem. Phys., 11, 6465–6474, doi:10.5194/acp-11-6465-2011, 2011.

Paatero, P. and Hopke, P. K.: Discarding or downweighting high-noise variables in factor analytic models, Anal. Chim. Acta, 490, 277–289, doi:10.1016/s0003-2670(02)01643-4, 2003.

Paatero, P. and Tapper, U.: Positive matrix factorization – a nonnegative factor model with optimal utilization of error-estimates of data values, Environmetrics, 5, 111–126, 1994.

Pathak, R.: Characteristics of aerosol acidity in Hong Kong, Atmos. Environ., 38, 2965–2974, doi:10.1016/j.atmosenv.2004.02.044, 2004.

Pathak, R. K., Yao, X., and Chan, C. K.: Sampling artifacts of acidity and ionic species in $PM_{2.5}$, Environ. Sci. Technol., 38, 254–259, doi:10.1021/es0342244, 2004.

ACPD
15, 18537–18576, 2015

Pathak, R. K., Wu, W. S., and Wang, T.: Summertime $PM_{2.5}$ ionic species in four major cities of China: nitrate formation in an ammonia-deficient atmosphere, Atmos. Chem. Phys., 9, 1711–1722, doi:10.5194/acp-9-1711-2009, 2009.

Quan, J., Zhang, Q., He, H., Liu, J., Huang, M., and Jin, H.: Analysis of the formation of fog and haze in North China Plain (NCP), Atmos. Chem. Phys., 11, 8205–8214, doi:10.5194/acp-11-8205-2011, 2011.

Schneider, J., Weimer, S., Drewnick, F., Borrmann, S., Helas, G., Gwaze, P., Schmid, O., Andreae, M. O., and Kirchner, U.: Mass spectrometric analysis and aerodynamic properties of various types of combustion-related aerosol particles, Int. J. Mass Spectrom., 258, 37–49, doi:10.1016/j.ijms.2006.07.008, 2006.

Setyan, A., Zhang, Q., Merkel, M., Knighton, W. B., Sun, Y., Song, C., Shilling, J. E., Onasch, T. B., Herndon, S. C., Worsnop, D. R., Fast, J. D., Zaveri, R. A., Berg, L. K., Wiedensohler, A., Flowers, B. A., Dubey, M. K., and Subramanian, R.: Characterization of submicron particles influenced by mixed biogenic and anthropogenic emissions using high-resolution aerosol mass spectrometry: results from CARES, Atmos. Chem. Phys., 12, 8131–8156, doi:10.5194/acp-12-8131-2012, 2012.

Sun, J., Zhang, Q., Canagaratna, M. R., Zhang, Y., Ng, N. L., Sun, Y., Jayne, J. T., Zhang, X., Zhang, X., and Worsnop, D. R.: Highly time- and size-resolved characterization of submicron aerosol particles in Beijing using an Aerodyne Aerosol Mass Spectrometer, Atmos. Environ., 44, 131–140, doi:10.1016/j.atmosenv.2009.03.020, 2010.

Sun, Y., Zhang, Q., Macdonald, A. M., Hayden, K., Li, S. M., Liggio, J., Liu, P. S. K., Anlauf, K. G., Leaitch, W. R., Steffen, A., Cubison, M., Worsnop, D. R., van Donkelaar, A., and Martin, R. V.: Size-resolved aerosol chemistry on Whistler Mountain, Canada with a high-resolution aerosol mass spectrometer during INTEX-B, Atmos. Chem. Phys., 9, 3095–3111, doi:10.5194/acp-9-3095-2009, 2009.

Sun, Y.-L., Zhang, Q., Schwab, J. J., Demerjian, K. L., Chen, W.-N., Bae, M.-S., Hung, H.-M., Hogrefe, O., Frank, B., Rattigan, O. V., and Lin, Y.-C.: Characterization of the sources and processes of organic and inorganic aerosols in New York city with a high-resolution time-of-flight aerosol mass apectrometer, Atmos. Chem. Phys., 11, 1581–1602, doi:10.5194/acp-11-1581-2011, 2011.

Sun, Y., Wang, Z., Dong, H., Yang, T., Li, J., Pan, X., Chen, P., and Jayne, J. T.: Characterization of summer organic and inorganic aerosols in Beijing, China with an aerosol chemical speciation monitor, Atmos. Environ., 51, 250–259, doi:10.1016/j.atmosenv.2012.01.013, 2012a.

ACPD
15, 18537–18576, 2015

Sun, Y. L., Zhang, Q., Schwab, J. J., Yang, T., Ng, N. L., and Demerjian, K. L.: Factor analysis of combined organic and inorganic aerosol mass spectra from high resolution aerosol mass spectrometer measurements, Atmos. Chem. Phys., 12, 8537–8551, doi:10.5194/acp-12-8537-2012, 2012b.

Sun, Y., Wang, Z., Fu, P., Jiang, Q., Yang, T., Li, J., and Ge, X.: The impact of relative humidity on aerosol composition and evolution processes during wintertime in Beijing, China, Atmos. Environ., 77, 927–934, doi:10.1016/j.atmosenv.2013.06.019, 2013a.

Sun, Y. L., Wang, Z. F., Fu, P. Q., Yang, T., Jiang, Q., Dong, H. B., Li, J., and Jia, J. J.: Aerosol composition, sources and processes during wintertime in Beijing, China, Atmos. Chem. Phys., 13, 4577–4592, doi:10.5194/acp-13-4577-2013, 2013b.

Sun, Y. L., Jiang, Q., Wang, Z. F., Fu, P. Q., Li, J., Yang, T., and Yin, Y.: Investigation of the sources and evolution processes of severe haze pollution in Beijing in January 2013, J. Geophys. Res.-Atmos., 119, 4380–4398, doi:10.1002/2014JD021641, 2014.

Ulbrich, I. M., Canagaratna, M. R., Zhang, Q., Worsnop, D. R., and Jimenez, J. L.: Interpretation of organic components from Positive Matrix Factorization of aerosol mass spectrometric data, Atmos. Chem. Phys., 9, 2891–2918, doi:10.5194/acp-9-2891-2009, 2009.

Wang, L. T., Wei, Z., Yang, J., Zhang, Y., Zhang, F. F., Su, J., Meng, C. C., and Zhang, Q.: The 2013 severe haze over southern Hebei, China: model evaluation, source apportionment, and policy implications, Atmos. Chem. Phys., 14, 3151–3173, doi:10.5194/acp-14-3151-2014, 2014.

Wang, X., Williams, B. J., Wang, X., Tang, Y., Huang, Y., Kong, L., Yang, X., and Biswas, P.: Characterization of organic aerosol produced during pulverized coal combustion in a drop tube furnace, Atmos. Chem. Phys., 13, 10919–10932, doi:10.5194/acp-13-10919-2013, 2013.

Wang, Z., Li, J., Wang, Z., Yang, W., Tang, X., Ge, B., Yan, P., Zhu, L., Chen, X., Chen, H., Wand, W., Li, J., Liu, B., Wang, X., Wand, W., Zhao, Y., Lu, N., and Su, D.: Modeling study of regional severe hazes over mid-eastern China in January 2013 and its implications on pollution prevention and control, Science China Earth Sciences, 57, 3–13, doi:10.1007/s11430-013-4793-0, 2014b.

Watson, J. G.: Visibility: science and regulation, JAPCA J. Air Waste Ma., 52, 628–713, doi:10.1080/10473289.2002.10470813, 2002.

ACPD
15, 18537–18576, 2015

Zhang, J. K., Sun, Y., Liu, Z. R., Ji, D. S., Hu, B., Liu, Q., and Wang, Y. S.: Characterization of submicron aerosols during a month of serious pollution in Beijing, 2013, Atmos. Chem. Phys., 14, 2887–2903, doi:10.5194/acp-14-2887-2014, 2014.

Zhang, Q., Canagaratna, M. R. Jayne, J. T., Worsnop, D. R., and Jimenez, J. L.: Time- and size-resolved chemical composition of submicron particles in Pittsburgh: implications for aerosol sources and processes, J. Geophys. Res., 110, D07S09, doi:10.1029/2004jd004649, 2005a.

Zhang, Q., Worsnop, D. R., Canagaratna, M. R., and Jimenez, J. L.: Hydrocarbon-like and oxygenated organic aerosols in Pittsburgh: insights into sources and processes of organic aerosols, Atmos. Chem. Phys., 5, 3289–3311, doi:10.5194/acp-5-3289-2005, 2005b.

Zhang, Q., Jimenez, J. L., Worsnop, D. R., and Canagaratna, M.: A case study of urban particle acidity and its influence on secondary organic aerosol, Environ. Sci. Technol., 41, 3213–3219, doi:10.1021/es061812j, 2007.

Zhao, X. J., Zhao, P. S., Xu, J., Meng„ W., Pu, W. W., Dong, F., He, D., and Shi, Q. F.: Analysis of a winter regional haze event and its formation mechanism in the North China Plain, Atmos. Chem. Phys., 13, 5685–5696, doi:10.5194/acp-13-5685-2013, 2013.

Zheng, B., Zhang, Q., Zhang, Y., He, K. B., Wang, K., Zheng, G. J., Duan, F. K., Ma, Y. L., and Kimoto, T.: Heterogeneous chemistry: a mechanism missing in current models to explain secondary inorganic aerosol formation during the January 2013 haze episode in North China, Atmos. Chem. Phys., 15, 2031–2049, doi:10.5194/acp-15-2031-2015, 2015a.

Zheng, G. J., Duan, F. K., Su, H., Ma, Y. L., Cheng, Y., Zheng, B., Zhang, Q., Huang, T., Kimoto, T., Chang, D., Pöschl, U., Cheng, Y. F., and He, K. B.: Exploring the severe winter haze in Beijing: the impact of synoptic weather, regional transport and heterogeneous reactions, Atmos. Chem. Phys., 15, 2969–2983, doi:10.5194/acp-15-2969-2015, 2015b.

ACPD
15, 18537–18576, 2015

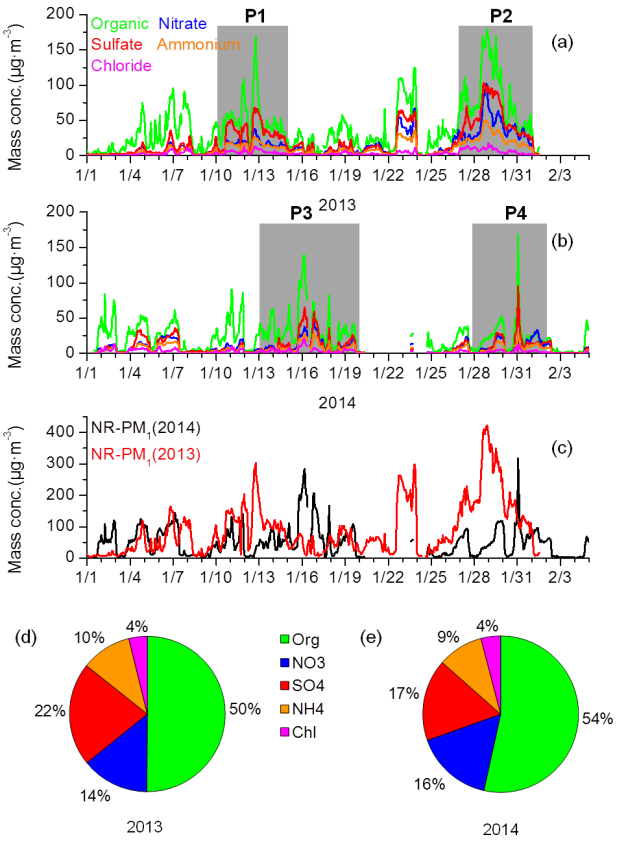

Figure 1. Time series of NR-PM_1 species concentrations in **(a)** January 2013 and **(b)** January 2014; **(c)** total NR-PM_1 mass concentration and NR-PM_1 chemical composition in **(d)** January 2013 and **(e)** January 2014. The P1 and P2 in **(a)** and P3 and P4 in **(b)**, which were showed as grey background, represent four pollution events in January 2013 and 2014.

ACPD
15, 18537–18576, 2015

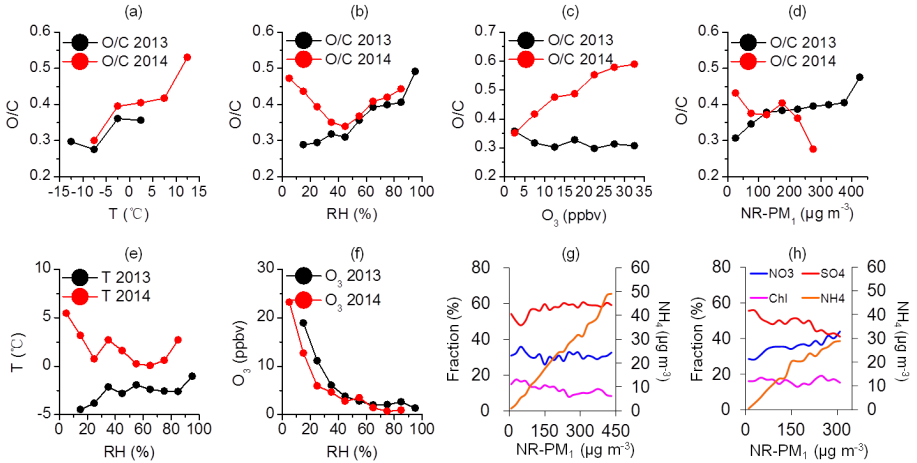

Figure 2. Variations of O/C ratios as a function of **(a)** temperature, **(b)** RH, **(d)** O_3, and **(d)** NR-PM_1 mass concentration in January 2013 and 2014; variations of **(e)** temperature and **(f)** O_3 as a function of RH in January 2013 and 2014; and the relative contribution of three acidic components (SO_4, NO_3 and Chl) to the total acid material and NH_4 as a function of NR-PM_1 mass concentrations in January **(g)** 2013 and **(h)** 2014.

ACPD
15, 18537–18576, 2015

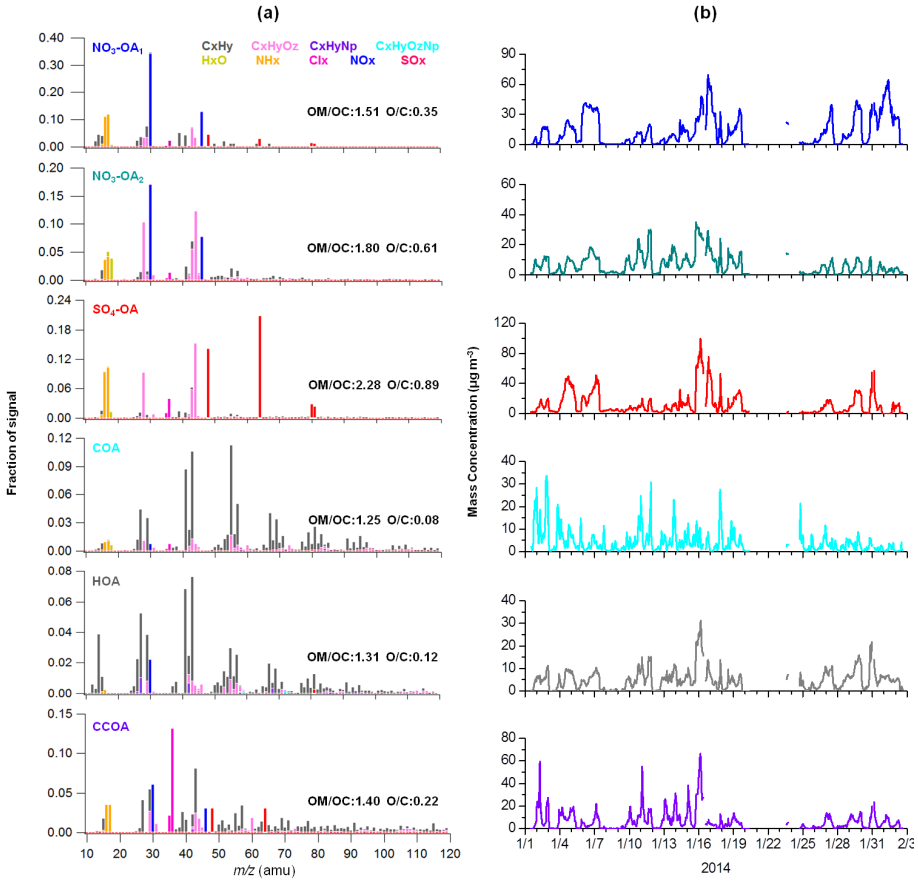

Figure 3. (a) The AMS m/z profiles and **(b)** time series of the six factors identified by the PMF analysis in January 2014.

ACPD
15, 18537–18576, 2015

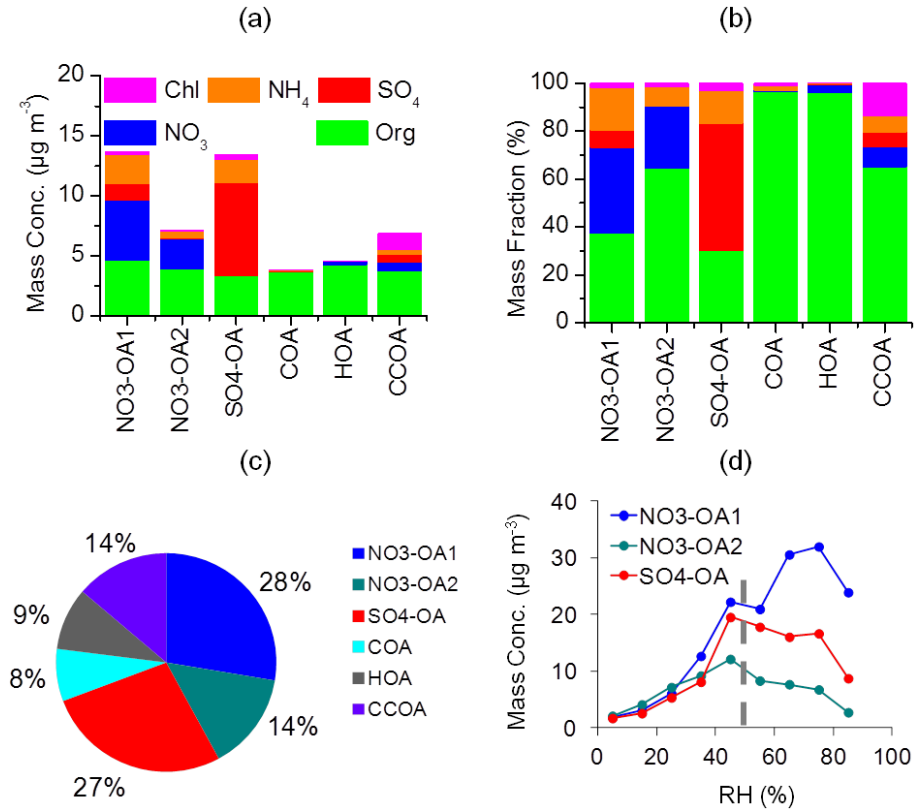

Figure 4. Chemical composition of the PMF factors in January 2014: **(a)** mass concentrations and **(b)** mass fractions of the NR-species (organics, sulfate, nitrate, ammonium and chloride) in each factor; **(c)** average composition of every PMF factor; and **(d)** variation in the two NO_3-OA factors and the SO_4-OA factor as a function of RH.

ACPD
15, 18537–18576, 2015

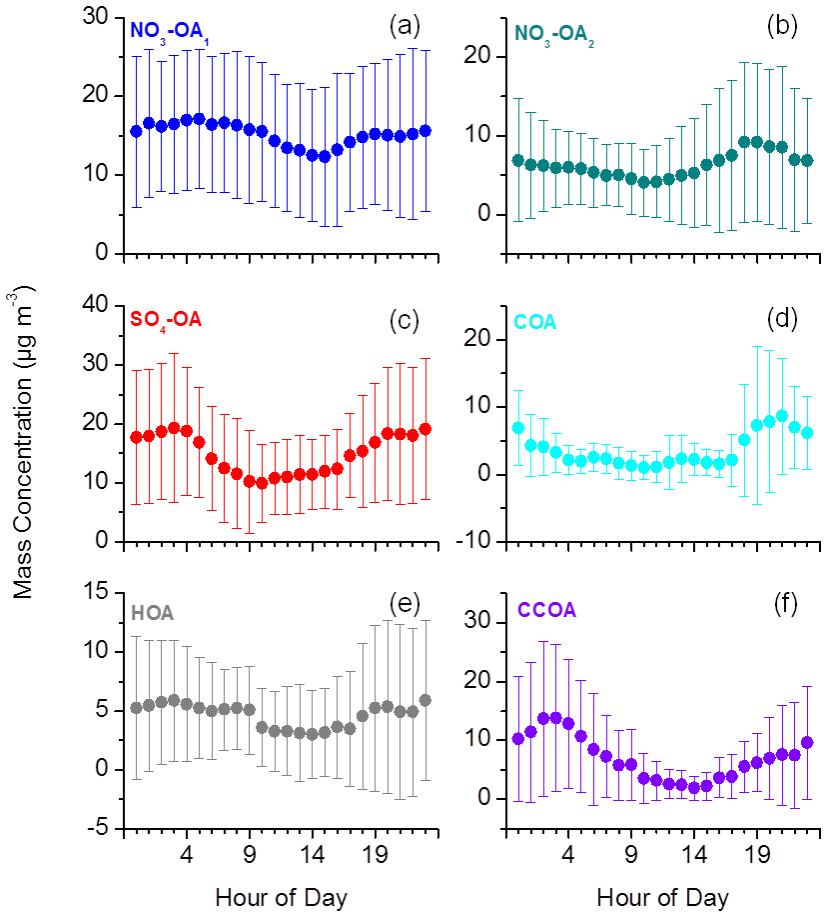

Figure 5. Diurnal cycles of the six PMF factors in January 2014: **(a)** NO_3-OA1; **(b)** NO_3-OA2; **(c)** SO_4-OA; **(d)** COA; **(e)** HOA; and **(f)** CCOA. The error bars indicate the standard deviation.

ACPD
15, 18537–18576, 2015

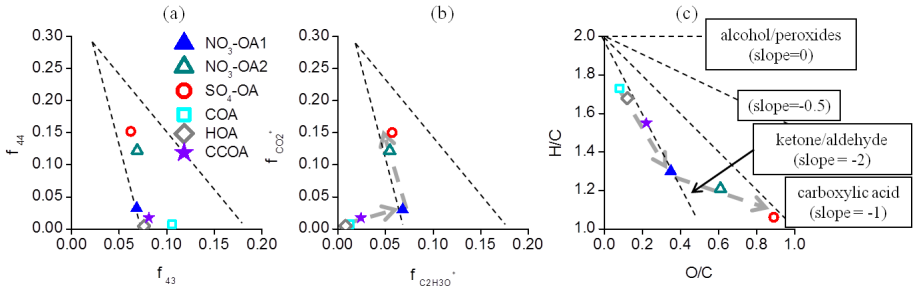

Figure 6. The **(a)** f_{44} (fraction of m/z 44 in OA) vs. f_{43} (fraction of m/z 43 in OA) and **(b)** $f_{CO_2^+}$ (fraction of CO_2^+ in OA) vs. $f_{C_2H_3O^+}$ (fraction of $C_2H_3O^+$ in OA) relationships for six OA factors. The dashed lines in (a) and (b) refer to a triangular region that encompasses ambient OOA factors determined from the PMF analyses of 43 AMS datasets (Ng et al., 2010). **(c)** Van Krevelen diagram for six OA factors. The dashed lines indicate the changes of H/C against O/C due to the addition of specific functional groups to an aliphatic carbon (Heald et al., 2010).

ACPD
15, 18537–18576, 2015

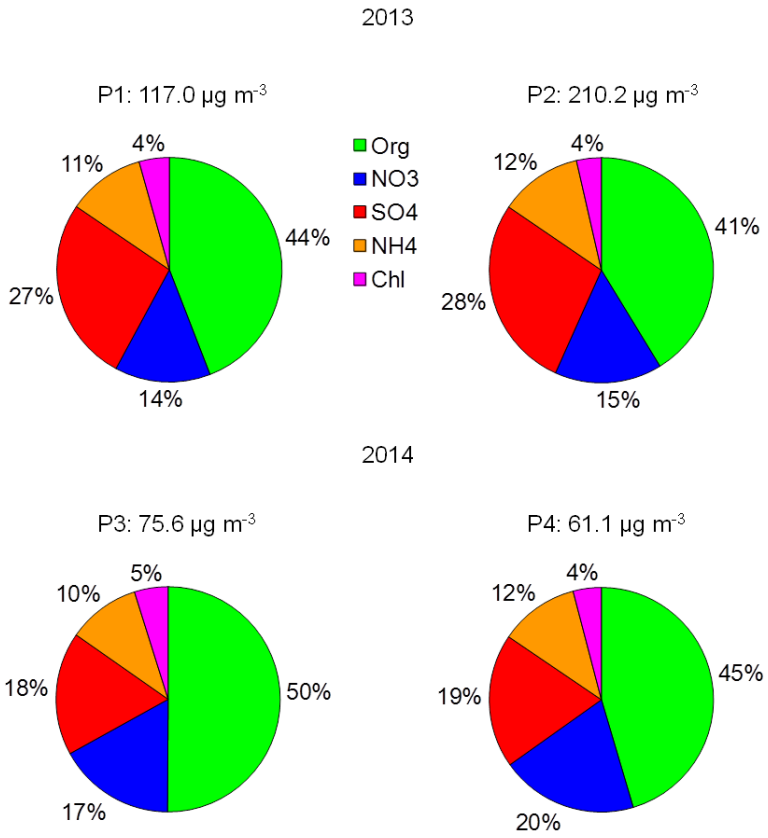

Figure 7. Average mass concentrations (above the pie charts) and chemical compositions of NR-PM_1 for the four heavy pollution periods. P1 and P1 represent two pollution events in January 2013, while P3 and P4 represent two pollution events in January 2014. They correspond to the four grey background periods in Fig. 1a and b.

ACPD
15, 18537–18576, 2015

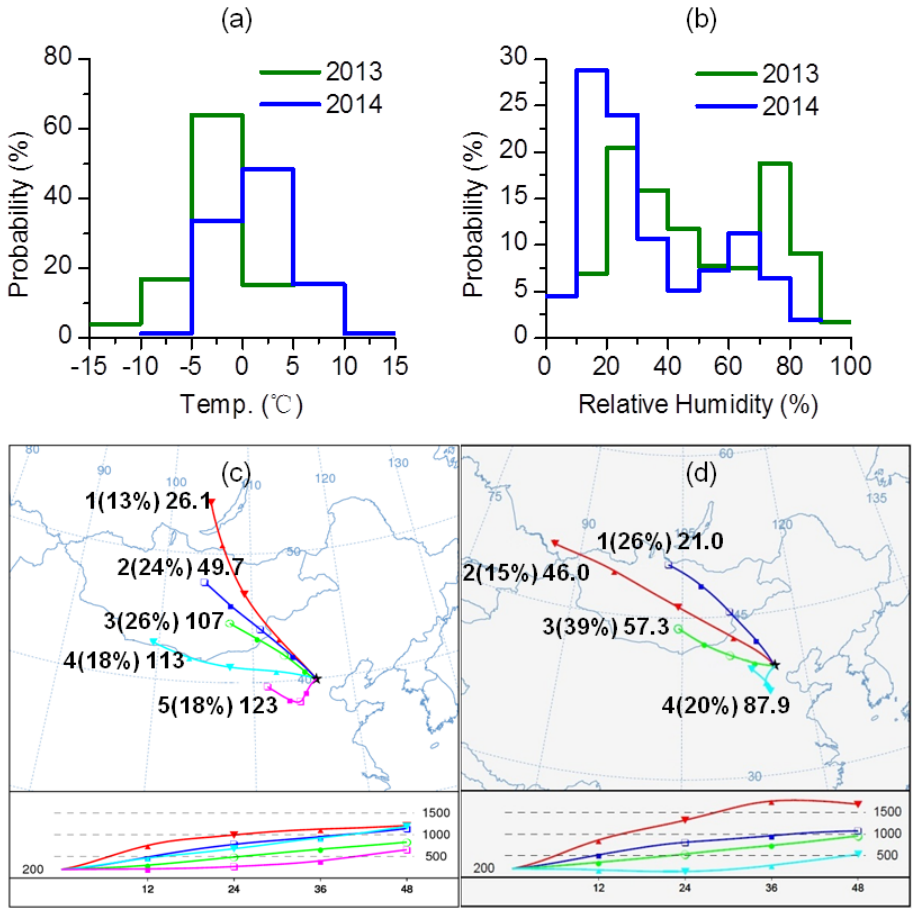

Figure 8. Probability of **(a)** temperature and **(b)** RH. Back trajectories for each of the identified clusters and corresponding cluster average NR-PM_1 concentration ($\mu g\,m^{-3}$) during the January **(c)** 2013 and **(d)** 2014 campaigns.

ACPD
15, 18537–18576, 2015

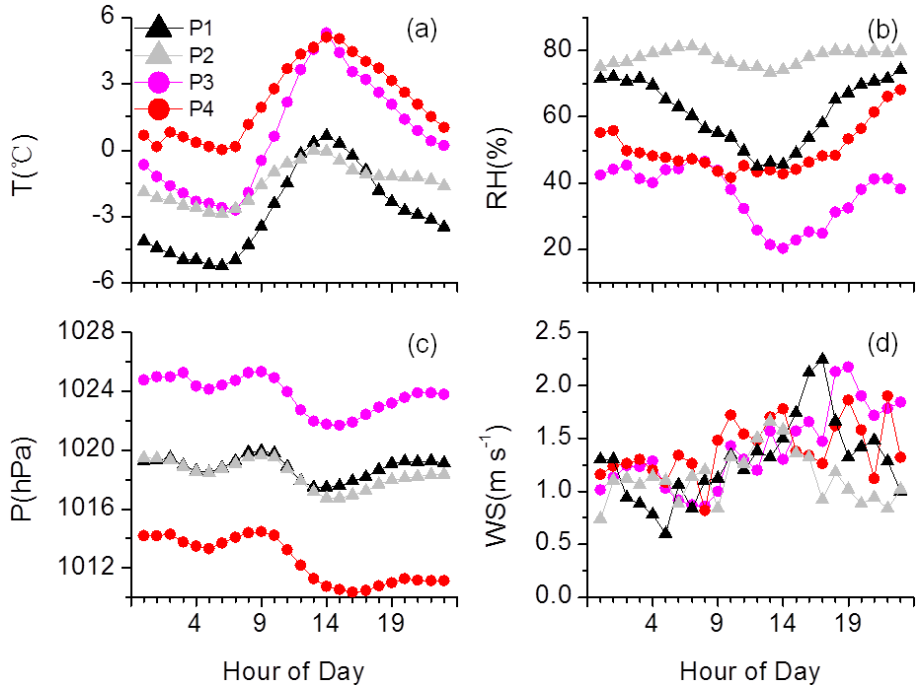

Figure 9. Diurnal profiles of meteorological factors for the four heavy pollution periods: **(a)** temperature; **(b)** relative humidity; **(c)** air pressure; and **(d)** wind speed.

ACPD
15, 18537–18576, 2015